Journal of Materials Chemistry

Cite this: J. Mater. Chem., 2012, 22, 20403

www.rsc.org/materials

PAPER

Structure–photovoltaic performance relationships for DSSC sensitizers having heterocyclic and benzene spacers†

Bo Hyung Kim[a] and Harold S. Freeman*[b]

Received 21st May 2012, Accepted 14th August 2012
DOI: 10.1039/c2jm33228k

Five new sensitizers based on different spacer groups were designed and synthesized in order to facilitate investigation of the effects of heterocyclic spacers on photovoltaic parameters in DSSCs. It was found that generic issues arising from the electronic nature of heterocyclic units affected voltage parameters, with **DP-P** giving the highest voltage. On the other hand, higher electron transfer yield across a wide range of the solar spectrum played an important role in enhanced current densities. Best performance was achieved by the thiophene based sensitizer **DP-T**, resulting in an efficiency of 3.5% with $J_{sc} = 8.19$ mA cm^{-2}, $V_{oc} = 0.618$ V, ff = 0.697.

Introduction

In recent decades, many metal-free organic dye sensitizers have been studied for their application in DSSCs (dye sensitized solar cells).[1] A typically employed structure is based on the push–pull system[2] (*i.e.* donor–spacer–acceptor system). In particular, double bond based spacers have been frequently introduced to give red-shifted absorption spectra aimed at large solar energy capture. However, widely employed C=C double bonds as spacers can limit DSSC efficiency, resulting in negative effects such as self-quenching of generated electrons by *cis–trans* isomerization[3] or aggregation.[4] Recently, the photovoltaic performance of a furan-based sensitizer (*versus* a thiophene-based sensitizer) was investigated with regard to recombination kinetics.[5] However, studies involving other heterocyclic ring systems as a spacer, in conjunction with the investigation of the effects of heterocyclic rings on photovoltaic parameters are little reported, limiting progress in the development of metal-free sensitizers for high efficiency DSSCs. Herein, we report on 1) the synthesis of novel metal-free sensitizers by systematic variation of the spacer unit (Fig. 1) and 2) intrinsic factors affecting photovoltaic performance through use of the resultant dyes in DSSCs.

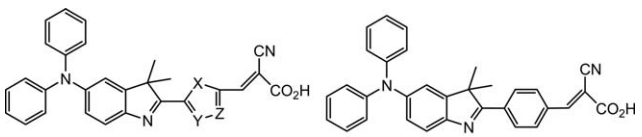

DP-T : X = S Y = CH Z = CH
DP-F : X = O Y = CH Z = CH
DP-TZ: X = S Y = N Z=CH
DP-P : X = N-CH_3 Y = CH Z=CH

DP-B

Fig. 1 Target molecular structures based on different spacers in a D–π–A system.

Experimental section

Materials

All reagents were purchased from Sigma-Aldrich, TCI, or Fisher Scientific. All chemicals were of reagent-grade quality and solvents purchased from commercial suppliers were used without further purification. Moisture-sensitive reactions were performed under either nitrogen or argon gas.

Characterizations

Structure confirmation. ^{1}H NMR and ^{13}C NMR spectra were recorded on a 300 MHz or 500 MHz Bruker Advance spectrometer using DMSO-d_6 or $CDCl_3$ as a solvent. High resolution mass spectra (HRMS) were obtained using electrospray ionization (ESI), in the positive mode, on an Agilent Technologies (Santa Clara, California) 6210 LC-TOF mass spectrometer.

Spectroscopic analysis. UV-Vis spectra in solution and on dye-loaded TiO_2 film were recorded on a Varian Cary 300 UV-Vis spectrophotometer. Photoluminescence of dye solutions was recorded using a fluorometer (Fluorolog®-3, HORIBA, USA) equipped with a 450 W xenon lamp (FL-1039/40, HORIBA, USA). The concentration of dye solutions used for emission

[a]*Fiber and Polymer Science Program, North Carolina State University, Raleigh, NC 27695, USA. E-mail: bkim6@ncsu.edu; Tel: +82-10-2597-2389*
[b]*Fiber and Polymer Science Program, North Carolina State University, Raleigh, NC 27695, USA. E-mail: hfreeman@ncsu.edu; Tel: +1-919-515-6552*

† Electronic supplementary information (ESI) available. See DOI: 10.1039/c2jm33228k

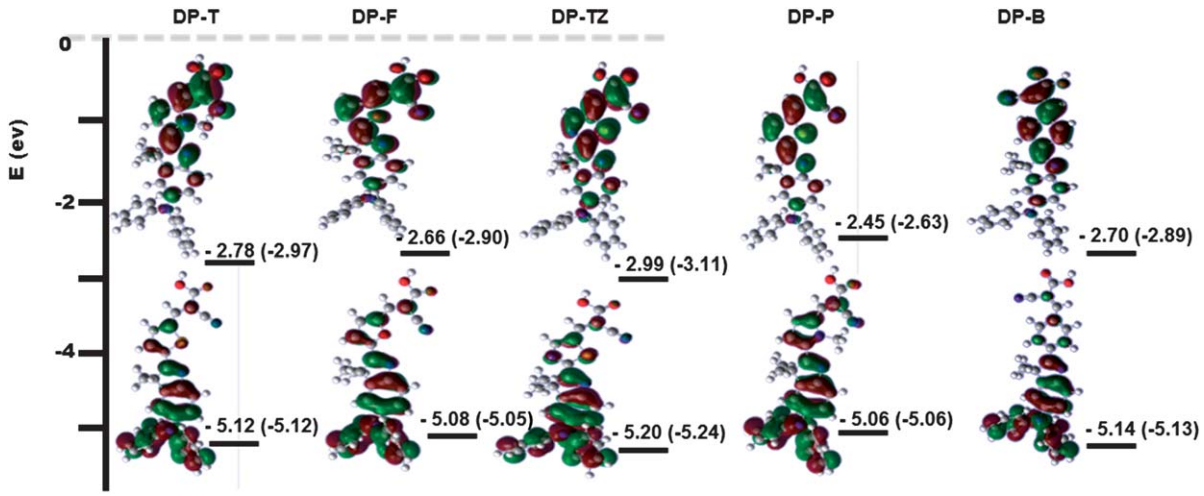

Fig. 2 Schematic representation of frontier orbital energies (upper; LUMO, bottom; HOMO, values in parenthesis were obtained with basis set of 6-31G(d)).

spectra was constrained to have absorbance of ~0.2. For amount of dye adsorbed on TiO_2 surfaces, dyes were extracted from TiO_2 films using 0.1 M NaOH in THF–H_2O (v/v, 1/1) followed by measurement of UV-Vis spectra and calculation of adsorbed amount of dye using the Beer–Lambert's law. Thickness of dye loaded TiO_2 film for all characterizations was 6 μm.

Electrochemical measurements. The oxidation potential of dye adsorbed on TiO_2 films was measured using a three electrode electrochemical cell in acetonitrile containing 0.1 M tetrabutylammonium hexafluorophosphate ($TBAPF_6$) at a scan rate of 100 mV s^{-1}. Dye coated TiO_2 film was used as a working electrode and Ag/Ag+ electrode and Pt wire were employed as a reference and counter electrode, respectively. The potential of the working electrode was calibrated using an Fc/Fc+ couple as an internal reference.

The impedance spectroscopy of the cell was recorded using an impedance analyzer connected to a potentiostat (reference 600TM, Gamry instruments, USA) in a frequency range of 0.1–105 Hz at room temperature under dark condition. The applied forward bias was −0.65 V and AC amplitude set to 10 mV.

Photovoltaic performance of DSSCs. Photocurrent–voltage characteristics of DSSCs were measured using a Keithley 2400 source meter under illumination of AM 1.5 G solar light coming from solar simulator (SOL3A, Oriel) equipped with a 450 W xenon lamp (91160, Oriel). The incident light intensity was calibrated using a reference Si solar cell (Newport Oriel, 91150V) to set 1 Sun (1 mW cm^{-2}). The current–voltage curve of the cell was obtained by applying external voltage bias and then measuring the generated photocurrent. The measurement was fully controlled under Oriel IV Test Station software. A mask (0.6 × 0.5 cm) was used to cover the testing cell during photocurrent and voltage measurements. The photo active area of cell was 0.5 × 0.4 cm.

IPCE (incident monochromatic photon to current conversion efficiency) experiments were carried out using a system (QEX10, PV Measurements, USA) equipped with a 75 W short arc xenon lamp (UXL-75XE, USHIO, Japan) as a light source connected to a monochromator. Calibration of incident light was performed using a silicone photodiode (IF035, PV Measurements). Monochromatic quantum efficiency was recorded at short circuit conditions under AC mode with white-light bias. Wavelength sampling interval was 10 nm. The beam size of monochromatic light illuminated on DSSCs was 0.1 × 0.5 cm and chopping speed of AC set to 10 Hz.

Synthesis of organic sensitizers

Synthesis of the target dyes **DP-T**, **DP-F**, **DP-TZ**, **DP-P**, and **DP-B** is described in Scheme 1. Synthetic details for **DP-T** and **DP-P** are reported elsewhere.[6]

(2*E*)-2-Cyano-3-(5-(5-(diphenylamino)-3,3-dimethyl-3*H*-indol-2-yl)furan-2-yl)acrylic acid (DP-F)

To a solution of compound **2d** (0.10 g, 0.25 mmol) and 2-cyanoacetic acid (0.03 g, 0.35 mmol) in acetonitrile (30 ml) was added a few drops of piperidine under N_2 gas flow. The reaction mixture was then stirred under reflux at 80 °C. The precipitate formed during reaction was collected by filtration and dried. Pure **DP-F** was obtained by column chromatography (DCM–methanol, 10/1, v/v) on silica gel, to give red solid. Yield: 29%, ^{1}H NMR (300 MHz, DMSO-d_6) δ = 7.83 (s, 1H), 7.49 (d, 1H, J = 8.4 Hz), 7.46 (d, 1H, J = 3.6 Hz), 7.35 (d, 1H, J = 3.6 Hz), 7.33–7.28 (m, 4H), 7.18 (d, 1H, J = 2.1 Hz), 7.07–7.01 (m, 6H), 6.92 (dd, 1H, J = 8.1 Hz, 2.1 Hz), 1.52 (s, 6H). ^{13}C NMR (500 MHz, DMSO-d_6) δ = 172.52, 162.80, 151.98, 150.90, 148.86, 147.97, 147.22, 145.93, 133.35, 129.48, 123.70, 123.42, 122.88, 121.38, 120.09, 118.19, 116.83, 115.54, 53.12, 22. 61. HRMS-ESI: calculated for $C_{30}H_{23}N_3O_3$ (M + H)/z 474.1812, found: 474.1806.

(2*E*)-2-Cyano-3-(2-(5-(diphenylamino)-3,3-dimethyl-3*H*-indol-2-yl)thiazol-5-yl)acrylic acid (DP-TZ)

DP-TZ was prepared using the same procedure as for **DP-F** except that **3d** was used as a starting material instead of **2d**. Pure **DP-TZ** was obtained by column chromatography

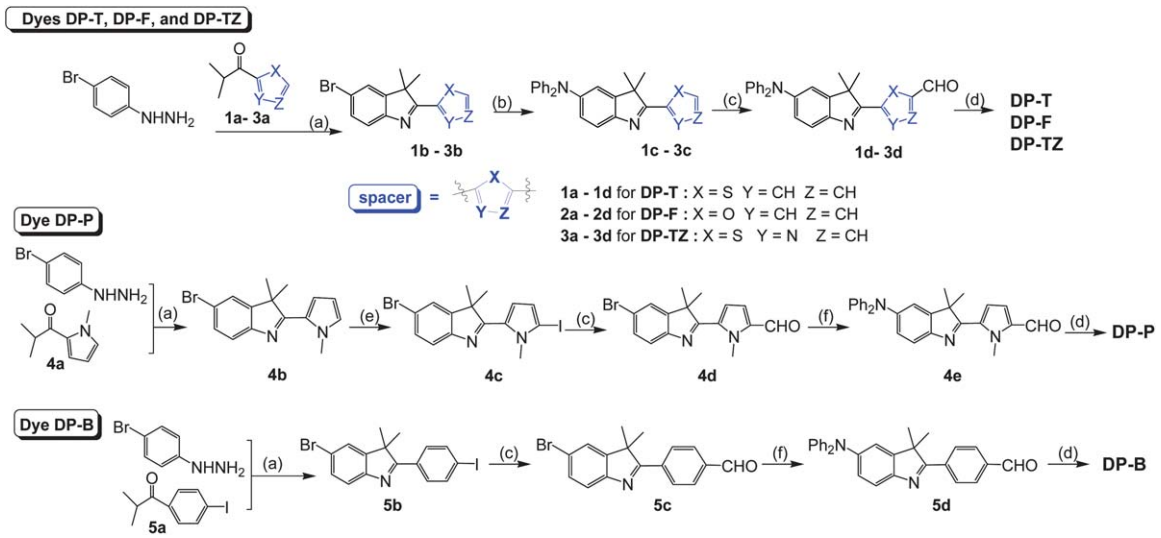

Scheme 1 Synthesis of target dyes. (a) TsOH·H2O, 85°C. (b) $Pd_2(dba)_3$, X-phos, sodium *tert*-butoxide, $NHPh_2$, toluene, reflux, 1 day. (c) (i) *n*-BuLi, THF, 0 °C to rt for 1 h; (ii) DMF, −78 °C, 1 h; (iii) −78 °C to rt for 2h; and (iv) 10 % HCl. (d) Cyanoacetic acid, piperidine (or NaOH), CH_3CN (or EtOH), reflux 3 h. (e) NIS, THF, rt, 4 h. (f) $Pd_2(dba)_3$, X-phos, Cs_2CO_3, sodium *tert*-butoxide, $NHPh_2$, toluene, reflux, 1 day.

(DCM–methanol, 11/1, v/v) on silica gel, to yield dark red solid. Yield: 49%, ^{1}H NMR (300 MHz, DMSO-d_6) δ = 8.55 (s, 1H), 8.18 (s, 1H), 7.62 (d, 1H, J = 8.4 Hz), 7.35–7.30 (m, 4H), 7.19 (d, 1H, J = 2.1 Hz), 7.09–7.04 (m, 6H), 6.95 (dd, 1H, J = 8.1 Hz, 2.1 Hz), 1.52 (s, 6H). ^{13}C NMR (500 MHz, DMSO-d_6) δ = 175.23, 164.34, 161.88, 151.12, 149.19, 147.60, 147.00, 137.24, 134.51, 129.60, 124.08, 123.42, 122.76, 122.29, 118.64, 116.25, 53.56, 23.24. HRMS-ESI: calculated for $C_{29}H_{22}N_4O_2S$ (M + H)/z 491.1536, found: 491.1536.

(2*E*)-2-Cyano-3-(4-(5-(diphenylamino)-3,3-dimethyl-3*H*-indol-2-yl)phenyl)acrylic acid (DP-B)

To a stirred solution of **5d** (0.05 g, 0.14 mmol) and 2-cyanoacetic acid (0.02 g, 0.27 mmol) in ethanol (10 ml) was added NaOH (0.005 g, 1.14 mmol) under N_2 gas flow. The reaction mixture was then stirred under reflux at 80 °C. The mixture formed during reaction was filtered and the product was dried. Pure **DP-B** was obtained by column chromatography (DCM–methanol, 10/1, v/v) on silica gel, to afford an orange solid. Yield: 36%, ^{1}H NMR (300 MHz, DMSO-d_6) δ = 8.25 (d, 2H, J = 8.4 Hz), 7.99 (d, 2H, J = 8.1 Hz), 8.00 (s, 1H), 7.56 (d, 1H, J = 8.1 Hz), 7.33–7.28 (m, 4H), 7.21 (d, 1H, J = 1.8 Hz), 7.06–7.02 (m, 6H), 6.94 (dd, 1H, J = 8.4 Hz, 2.1 Hz), 1.50 (s, 6H). ^{13}C NMR (500 MHz, DMSO-d_6) δ = 180.44, 162.85, 149.60, 148.13, 147.36, 146.72, 145.88, 134.81, 134.25, 129.63, 129.47, 128.29, 123.59, 122.82, 121.42, 118.82, 117.14, 53.08, 23.90. HRMS-ESI: calculated for $C_{32}H_{25}N_3O_2$ (M + H)/z 484.2020, found: 484.2017.

Fabrication of DSSCs[7]

To prepare a porous TiO_2 electrode, an FTO glass plate (F-doped SnO_2, TEC-8, 8 Ω, Pilkington, USA, 2.2 mm thick) was cleaned in a detergent solution using an ultrasonic bath, for 15 min, followed by rinsing with water and ethanol. Residual contaminants were removed by heating the cleaned FTO glass at 400 °C for 20 min. A layer of TiO_2 anatase nanoparticles (Ti-Nanoxide D/SP, Solaronix, Switzerland) was first coated on the FTO, pretreated with Ti(IV) bis(ethylacetoacetato)-diiso-propoxide solution (7.5% in BuOH), using a doctor-blade method. After drying the film at 120 °C, a scattering layer of TiO_2 nanoparticles (Ti-Nanoxide R/SP, Solaronix, Switzerland) was deposited and then gradually heated in air at 325 °C for 5 min, at 375 °C for 5 min, at 450 °C for 15 min, and sintered at 500 °C for 15 min. The resulting thin film was composed of a 12 μm thick TiO_2 nanocrystalline layer and a 6 μm thick scattering layer. The nanoporous TiO_2 electrode was immersed into 0.3 mM dye solution in THF and kept at room temperature 24 h to give adsorption of dye onto the TiO_2 surface. Coadsorbate of 1 mM DCA (deoxycholic acid) was added. A platinized electrode was prepared by placing a drop of H_2PtCl_6 solution (2 mg Pt in 1 ml ethanol) on punctured FTO and subsequent heating at 400 °C for 15 min. The dye loaded TiO_2 electrode and thermally platinized counter electrode were sealed together with a 60 μm hot-melt gasket (Suryln 1702, Dupont). After injecting electrolyte into cell by vacuum backfilling, the cell was again encapsulated using sealant (Suryln 1702, Dupont, 60 μm thick) and a cover glass. An electrolyte was employed for performance measurement of the DSSCs, which were composed of 0.6 M DMPII (1,2-dimethyl-3-*n*-propylimidazolium iodide), 0.1 M LiI, 0.05 M I_2 in anhydrous acetonitrile (anhyd. AN). An N719 dye mediated DSSC was fabricated as a reference cell for device measurements, where a 0.3 mM dye solution in ethanol was used and the electrolyte composition was 0.1 M LiI, 0.05 M I_2 or 0.6 M DMPII (1,2-dimehtyl-3-*n*-propylimidazolium iodide), 0.1 M LiI, 0.05 M I_2, 0.5 M TBP (4-*tert* butyl pyridine) in anhyd. AN.

Results and discussions

The target dyes are composed of a diphenylamine substituted indole moiety and cyanoacrylic acid group connected by 5 different spacers including thiophene, furan, thiazole, *N*-methyl pyrrole, and benzene (Fig. 1). Twisted non-planar geometry

between DPA (diphenylamine) and the conjugated unit was intended to aid charge separation[8] after photo-excitation of dyes. Following modeling studies to confirm a sufficient driving force for electron injection for all five dyes, target dyes were synthesized (Scheme 1) by reaction[9] of formylated intermediates (**1d**–**5d**) with cyanoacetic acid. Compounds **1b**–**5b** were prepared from the 4-bromophenyl hydrazine and 2-isobutyryl substituted heterocyclic (or iodo substituted benzene) intermediates (**1a**–**5a**) by the Fisher indole cyclization.[10] Subsequent C–N coupling of **1b**–**3b** with diphenylamine under Buchwarld–Hartwig conditions[11] produced intermediates **1c**–**3c**. In order to make formylated **1d**–**3d**, organometallation[12] was used. Dyes **DP-P** and **DP-B** were prepared using the same method as for dyes **DP-T**, **DP-F**, and **DP-TZ** with the use of iodinated intermediates (*e.g.* **5b**) instead of protonated intermediates for the formylation step. The use of iodinated intermediates was aimed at subsequent halogen–metal exchange, since the α-proton of *N*-methyl pyrrole and *para*-proton of benzene are not acidic enough to undergo deprotonation by *n*-BuLi.

Frontier orbital energies (Fig. 2) were calculated using DFT (density function theory)[13] from which B3LYP and 3-21G(d) or 6-31G(d) were adopted as the exchange correlation functional[14] and a basis set, respectively. Using the small or expanded basis set, frontier orbital energies decreased in the order of *N*-methyl pyrrole > furan > thiophene > thiazole based dye. Considering delocalization energies of heterocyclic ring of thiazole (25 kcal mol^{-1}), thiophene (29 kcal mol^{-1}), pyrrole (21 kcal mol^{-1}), and furan (16 kcal mol^{-1}) compared to benzene (36 kcal mol^{-1}),[15] introduction of simple five-membered heterocyclic linkers in the molecular structures was expected to impart not only a more negative shift in the first excited state but also efficient charge transfer relative to the benzene spacer.[16] Despite the higher delocalization energy of pyrrole relative to that of furan, the more negative HOMO/LUMO level of pyrrole-based dye may be attributed to the reduced electron pulling ability of this moiety due to its electron-rich nature, thus increasing the HOMO/LUMO energy level. On the other hand, the lowest LUMO of the thiazole based dye, which has 25 kcal mol^{-1} of delocalization energy for thiazole ring, may be responsible for the strongest electron pulling effect of thiazole rings introduced as the π component in a D–π–A system.[17] From the isodensity surface plot of frontier orbitals (Fig. 2), it was found that the HOMO–LUMO excitation moved the electron distribution from the amino- substituted indole moiety to the cyanoacetic acid group for all dyes, imparting efficient charge separation.

TDDFT (time dependent density functional theory)[18] calculations were performed with parameters of BHandH/3-21G(d)//B3LYP/3-21G(d). Among the two main transitions shown (Table 1), excitation of the HOMO → LUMO transition results in the $S_0 \rightarrow S_1$ transition whereas $S_0 \rightarrow S_2$ transition mainly corresponded to the HOMO-1 → LUMO transition. Based on electron configurations shown at each electronic level (ESI, Fig. S1 and Table S1†), the $S_0 \rightarrow S_1$ transition was assigned to the ICT (internal charge transfer) band while the $S_0 \rightarrow S_2$ transition was considered as a localized π–π* transition. Since the ICT band is crucial to light harvesting in the conversion of photon energies to electricity in a DSSC system, calculated results corresponding to the $S_0 \rightarrow S_1$ transition were compared with experimental results. Except for the slightly overestimated λ_{max} of **DP-P**, computed λ_{max} trends among dyes followed those based on the experimental values. Bearing in mind that polarization effects and diffusion functions are important in excited state calculations, BHandH/6-31 + G(d,p)//B3LYP/6-31G(d), BHandH/6-31G(d,p)//B3LYP/6-31G(d), and BHnadH/6-31G(d)//B3LYP/6-31G(d) levels were performed (ESI, Table S2†). While the use of a higher level basis set did not cause a significant change in frontier orbital energy values, the use of BHandH/6-31 + G(d,p)//B3LYP/6-31G(d) significantly overestimated absorption maxima, unlike BHandH/3-21G(d)//B3LYP/3-21G(d). Despite involving a smaller basis set, TDDFT calculations using the BHandH hybrid functional are suitable for the quick prediction of ICT bands, with minimal deviation from the experimental values. The experimentally recorded λ_{max} values observed in the visible region were consistent with the generic electronic characteristic (electron rich or deficient) of heterocyclic rings employed in a D–π–A system.

However, absorption spectra for dye-loaded TiO_2 films were characterized by somewhat different behavior from those in solution (Fig. 3). Once dyes were adsorbed on the TiO_2 surface, they showed the following behaviors: (1) broadening of absorption spectrum and (2) shift in λ_{max} toward longer wavelengths to different degrees depending on the dye structure. The broadened spectra of dye-loaded TiO_2 films have been attributed to dye–dye and/or dye–TiO_2 interactions.[19] Unfortunately, the λ_{max} of **DP-P**

Table 1 Optical and electrochemical properties of dyes

λ_{cal}[a] [nm]								
$S_0 \rightarrow S_1$	$S_0 \rightarrow S_2$	Dyes	λ_{max}[b] [nm]	ε_{max}[b] [M^{-1} cm^{-1}]	λ_{max_emi}[b] [nm]	$\lambda_{max\_TiO_2}$[c] [nm]	E_{ox}[d] [V] *vs.* NHE[e]	E^*_{ox}[e] [V] *vs.* NHE
466	330	**DP-T**	353, 464	17 364, 25 491	621	476	1.389	−0.920
464	331	**DP-F**	343, 453	18 433, 22 086	611	474	1.342	−1.020
478	328	**DP-TZ**	349, 480	17 065, 25 931	642	499	1.437	−0.793
432	325	**DP-P**	307, 395	N/A, 17 062	576	N/A	N/A	N/A
423	304	**DP-B**	311, 435	31 955, 22 905	608	436	1.369	−1.062

[a] Calculated electronic transition energies with PCM-TD-BHandH/3-21G(d)//B3LYP/3-21G(d) level. [b] Absorption and emission spectra were recorded in THF. [c] Absorption spectra of dye-loaded TiO_2 film. [d] Oxidation potentials were measured from three electrode electrochemical cell in CH_3CN containing 0.1 M $TBAPF_6$ at a scan rate of 100 mV S^{-1}. Dye-loaded TiO_2 film, Ag/Ag+, and Pt wire were used as working, reference, and counter electrode, respectively. [e] Excited state oxidation potential obtained from $E_{ox} - E_{0\text{-}0}$ where $E_{0\text{-}0}$ was estimated from the intercept of absorption and emission spectra.

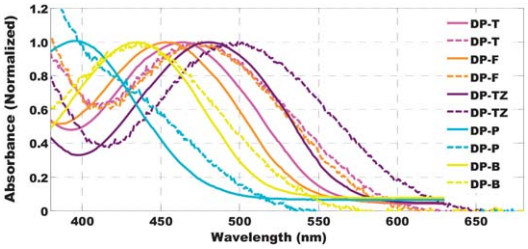

Fig. 3 Absorption spectra of dyes and dye-loaded TiO_2 films (line; absorption of dyes recorded in THF solution, dashed line; absorption of dye loaded TiO_2 films).

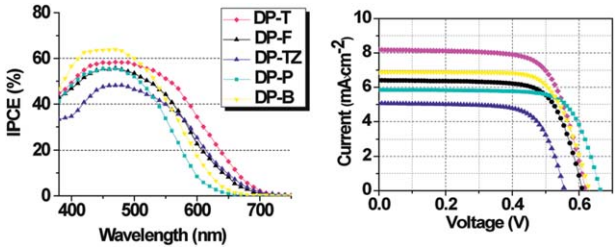

Fig. 4 IPCE spectra (left) and *I–V* curves (right) for DSSCs based on the present dyes.

on TiO_2 surface could not be resolved due to the overlap of its absorption band with that of the bare TiO_2 layer (ESI, Fig. S2†). Judging from the red shift of dyes **DP-T**, **DP-F**, and **DP-TZ** on TiO_2 film, they behave like J-aggregates on TiO_2. It is interesting to note that benzene based **DP-B** gave an unchanged λ_{max} while furan based **DP-F** and **DP-TZ** gave a relatively large shift in λ_{max}. The λ_{max} values of **DP-TZ** and **DP-F** on the TiO_2 surface shifted closer to the values obtained in solution following the addition of DCA (deoxycholic acid),[20] which is known to suppress dye aggregation (ESI, Fig. S3†). Results of previous research indicated that the smaller λ_{max} shifts associated with dyes from solution *versus* the solid state suggest a smaller tendency to form dye aggregates on the semiconductor surface.[1k,21] Based on this assumption, **DP-B**, showing the smallest change of absorption spectrum on TiO_2, seemed to be more efficient in suppressing the formation of dye aggregates on the TiO_2 surface.

Redox potentials of dye-loaded TiO_2 films (Table 1) showed the same trends as the electronic energies predicted from modeling studies (Fig. 2). E^*_{ox} values of all dyes were higher than the energy of the conduction band edge of TiO_2 (−0.5 V *versus* NHE).[22] Also, oxidation potentials were located below the energy of redox electrolyte I^-/I_3^- (0.42 V *versus* NHE).[22] As a result, enough driving force for both electron injection and regeneration of oxidized dyes was obtained during the operation of DSSCs.

Photovoltaic performance was measured under simulated AM 1.5 G irradiation. All photovoltaic parameters are listed in Table 2.

Taking into consideration the effect of sensitizer structures on photovoltaic performances, current density of the device increased in the order of sensitizer having thiazole (5.06 mA cm^{-2}) < *N*-methyl pyrrole (5.85 mA cm^{-2}) < furan (6.40 mA cm^{-2}) < benzene (6.89 mA cm^{-2}) ≪ thiophene (8.19 mA cm^{-2}) spacer. Current density is a result of the product of LHE (light harvesting efficiency), electron injection efficiency, and electron collecting efficiency.[1k,23] Assuming LHE to be unity for all sensitizers at ε_{max} of 17 000–25 931, the magnitude of driving force, which is related to the electron injection efficiency[17,24] increased in the order of *N*-methyl pyrrole, benzene > furan > thiophene > thiazole. However, this does not fully account for the observed orders in short circuit currents. Therefore, IPCE (incident photon-to current conversion efficiency) curves (Fig. 4) were recorded to further explain the obtained current densities obtained, since short circuit current is a reflection of current density converted from incident photon at a given wavelength.

Table 2 Photovoltaic performance[a] and charge recombination lifetimes of DSSCs sensitized with the present dyes

Dyes	J_{sc}/[mA cm^{-2}]	V_{oc}/[mV]	ff	η/[%]	τ^b/[ms]
DP-T	8.19	618	0.697	3.53	8.0
DP-F	6.40	609	0.717	2.80	3.2
DP-TZ	5.06	555	0.709	1.99	1.0
DP-P	5.85	664	0.738	2.86	40.0
DP-B	6.89	627	0.715	3.09	15.9

[a] *Conditions*: AM 1.5 G (100 mW cm^{-2}) was irradiated on the testing cells (working area of 0.20 cm^2). Electrolyte composition was 0.6 M DMPII, 0.1 M LiI, 0.05 M I_2 in anhy. AN. [b] Charge recombination lifetimes were extracted from a Nyquist plot of impedance measurements.

It is interesting to note that the maximum quantum efficiency at a given λ_{max} did not follow the trends shown in current densities. To be specific, IPCE plateau increased in the following order: device sensitized by benzene > thiophene > furan ≈ *N*-methyl pyrrole > thiazole based dyes. This relative lower (or higher) plateau could be due to the reduction (or increase) in electron transfer yield.[1k] For example, somewhat the lowered plateaus from **DP-F** despite a high driving force for electron injection and high E_{max} might arise from dye aggregation behavior on the TiO_2 surface, decreasing electron injection yield. This assumption is consistent with the absorption curve for a **DP-F** loaded TiO_2 film, which showed the largest spectral shift relative to that in solution. Current density of the device based on **DP-F** increased ~8% by the addition of DCA (ESI, Fig. S4†). On the other hand, the device constructed from **DP-B** resulted in the highest plateau. This finding further supports aggregation behavior as a factor affecting IPCE plateaus. Nonetheless, the highest electron transfer yield from the **DP-B** based device did not give the highest current density, due to solar energy capture in a narrower region of the solar spectrum than the **DP-T** based device.

Concerning the voltage parameters measured, a good correlation was found between observed voltages and electronic nature of the sensitizers. Open circuit voltage (V_{oc}) can be determined from the potential difference between the conduction band edge of TiO_2 and redox species in electrolyte as shown in the equation below, which also shows the dependence of V_{oc} on the electron density (n) on TiO_2 semiconductor:[25]

$$V_{oc} = E_{red} - E_{cb} - \gamma \frac{k_B T}{e} \ln\left(\frac{N_e}{n}\right)$$

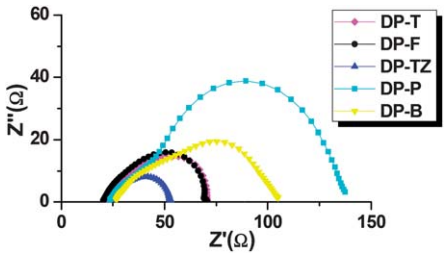

Fig. 5 Nyquist phase plot based on DSSCs sensitized with the present dyes (EIS measurements were performed under dark condition with a forward bias of −0.65 V and AC amplitude set to 10 mV.

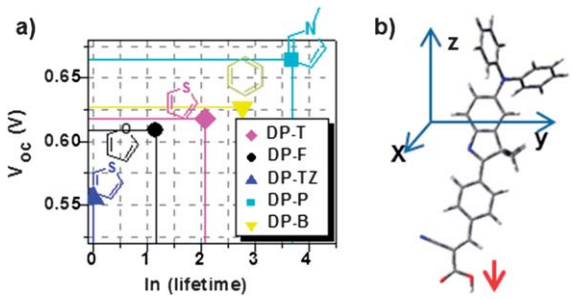

Fig. 6 (a) Plot of V_{oc} for DSSCs based on sensitizers having different spacers as a function of lifetime from EIS measurements. (b) Representation of coordinates for the calculation of normal dipole moment (μ_{normal}).

where γ is a characteristic constant of TiO_2 tailing states, k_B is Boltzmann constant, T is absolute temperature, e is elementary charge, and N_e is the effective density states at E_{cb} edge. In this context, an assumption was made that the E_{redox} of electrolyte is the same for all devices under similar DSSC fabrication conditions. Consequently, charge recombination, which can affect electron density in TiO_2, seems to significantly affect V_{oc}. Specifically, charge recombination lifetimes (τ) of devices extracted from EIS measurements (Table 2 and Fig. 5) showed the following order: a device sensitized with dyes having *N*-methyl pyrrole (40 ms) > benzene (16 ms) > thiophene (8 ms) > furan (3 ms) > thiazole (1 ms) unit. This order strongly correlated with V_{oc} values of 0.664 V, 0.627 V, 0.618 V, 0.609 V, and 0.555 V for **DP-P**, **DP-B**, **DP-T**, **DP-F**, and **DP-TZ**, respectively (*cf.* Fig. 6a).

Table 3 Predicted polarizabilities, dipole moments[a], and relative adsorbed amounts of dyes

Cal. values	DP-T	DP-F	DP-TZ	DP-P	DP-B
μ_{normal} [Debye]	−4.97	−5.27	−4.30	−2.88	−3.42
Polarizability [Bohr^3]	458.9	429.6	467.6	443.7	458.8
Rel. ads. amount[b]	1	0.91	0.79	0.62	0.80

[a] All parameters were obtained by single point calculations after geometry optimization using DFT-B3LYP with3-21G(d). μ_{normal} was dipole moment of isolated dyes at the direction perpendicular to the plane of TiO_2 surface (*cf.* Fig. 6b). [b] Relative adsorbed amounts of dyes were obtained by applying dyes on TiO_2 film from 0.1 M NaOH in THF–H_2O (v/v, 1 : 1). The value for **DP-T** was referenced for the comparison.

In order to investigate the origin of different τ values among dyes, normal dipole moments (μ_{normal}) as well as polarizabilities were calculated. In addition, relative adsorbed amounts of dyes on TiO_2 were measured by dissolving dyes adsorbed on TiO_2 in a basic solution (Table 3).

In view of results from related research,[26,27] our expectation was that the higher the level of dye loading in the ordered form, the longer the electron lifetime, due to surface blocking of dye molecules from the TiO_2 vacant sites. In addition, the higher the polarizability of dye, the higher the concentration of local oxidizing species, increasing interactions between electrons on TiO_2 and oxidizing species in the electrolyte. From the calculated results, τ values seem to closely correlate with polarizability and/or electron deficient nature of heterocyclic rings rather than μ_{normal}, except for the device based on **DP-F**. In this regard, the device based on **DP-P** imparting lowest polarizabilities gave the highest lifetimes. The reason for the somewhat lower lifetime for the **DP-F** based device is still unclear, considering the relatively low polarizability and electron rich character of this dye.

Furthermore, **DP-F** gave high loads on the TiO_2 surface. It seems that the efficient blocking of dyes on the TiO_2 electrode remains a factor in the observed τ among dyes. Although we would not expect exact alignment of the present dye molecules on the porous TiO_2 semiconductor surface, it can be concluded that the alignment of **DP-F** on the TiO_2 surface does not permit efficient packing, resulting in a low V_{oc}. As a result, high dye loads in conjunction with a highly ordered packing of dyes would provide increased τ and a high efficiency DSSC.

Conclusions

Structure–performance relationships in DSSCs were investigated *via* systematic spacer changes in a D–π–A system. Based on current–potential curves, current density increased in the order **DP-TZ** < **DP-P** < **DP-F** < **DP-B** < **DP-T** The highest plateau of quantum efficiency from IPCE spectra was obtained from **DP-B**, indicating a relationship between decreased (or increased) aggregation behavior of dyes on a TiO_2 surface and higher (or lower) electron transfer yield. The dependence of open-circuit voltage on electron lifetime was evident, resulting in enhanced V_{oc} in the order of devices based on **DP-TZ** < **DP-F** < **DP-T** < **DP-B** < **DP-P**. The lower polarizabilities of the molecules contributed to increased lifetimes but this benefit was weakened when efficient surface blocking was reduced, resulting in an unexpected drop in open-circuit voltage for **DP-F**. In order to unveil the precise nature of the surface blocking behavior of dyes in DSSCs, a 3-dimensional modeling study of dyes in the TiO_2 slab is needed.

References

1 (*a*) K. Sayama, K. Hara, N. Mori, M. Satsuki, S. Suga, S. Tsukagoshi, Y. Abe, H. Sugihara and H. Arakawa, *Chem. Commun.*, 2000, 1173; (*b*) K. Hara, T. Sato, R. Katoh, A. Furube, Y. Ohga, A. Shinpo, S. Suga, K. Sayama, H. Sugihara and H. Arakawa, *J. Phys. Chem. B*, 2002, **107**, 597; (*c*) K. Hara, M. Kurashige, Y. Dan-oh, C. Kasada, A. Shinpo, S. Suga, K. Sayama and H. Arakawa, *New J. Chem.*, 2003, **27**, 783; (*d*) K. Hara, M. Kurashige, S. Ito, A. Shinpo, S. Suga, K. Sayama and H. Arakawa, *Chem. Commun.*, 2003, 252; (*e*) T. Kitamura, M. Ikeda, K. Shigaki, T. Inoue, N. A. Anderson, X. Ai, T. Lian and S. Yanagida, *Chem. Mater.*,

2004, **16**, 1806; (*f*) L. Schmidt-Mende, U. Bach, R. Humphry-Baker, T. Horiuchi, H. Miura, S. Ito, S. Uchida and M. Grätzel, *Adv. Mater.*, 2005, **17**, 813; (*g*) S. Hwang, J. H. Lee, C. Park, H. Lee, C. Kim, C. Park, M.-H. Lee, W. Lee, J. Park, K. Kim, N.-G. Park and C. Kim, *Chem. Commun.*, 2007, 4887; (*h*) S. Ito, H. Miura, S. Uchida, M. Takata, K. Sumioka, P. Liska, P. Comte, P. Pechy and M. Gratzel, *Chem. Commun.*, 2008, 5194; (*i*) S. Qu, W. Wu, J. Hua, C. Kong, Y. Long and H. Tian, *J. Phys. Chem. C*, 2010, **114**, 1343; (*j*) C. Teng, X. Yang, C. Yang, S. Li, M. Cheng, A. Hagfeldt and L. Sun, *J. Phys. Chem. C*, 2010, **114**, 9101; (*k*) C. Teng, X. Yang, C. Yang, H. Tian, S. Li, X. Wang, A. Hagfeldt and L. Sun, *J. Phys. Chem. C*, 2010, **114**, 11305.

2 R. Chen, G. Zhao, X. Yang, X. Jiang, J. Liu, H. Tian, Y. Gao, X. Liu, K. Han, M. Sun and L. Sun, *J. Mol. Struct.*, 2008, **876**, 102.

3 Y. Onganer, M. Yin, D. R. Bessire and E. L. Quitevis, *J. Phys. Chem.*, 1993, **97**, 2344.

4 (*a*) K. Norland and A. Ames, *Photogr. Sci. Eng.*, 1970, **14**, 295; (*b*) C. Reich, W. D. Pandolfe and G. R. Bird, *Photogr. Sci. Eng.*, 1973, **17**, 334.

5 J. T. Lin, P.-C. Chen, Y.-S. Yen, Y.-C. Hsu, H.-H. Chou and M.-C. P. Yeh, *Org. Lett.*, 2008, **11**, 97.

6 B. Kim, PhD thesis, North Carolina State University, 2012.

7 S. Ito, T. N. Murakami, P. Comte, P. Liska, C. Grätzel, M. K. Nazeeruddin and M. Grätzel, *Thin Solid Films*, 2008, **516**, 4613.

8 (*a*) N. Hirata, J. J. Lagref, E. J. Palomares, J. R. Durrant, M. K. Nazeeruddin, M. Gratzel and D. Di Censo, *Chem.–Eur. J.*, 2004, **10**, 595; (*b*) H. Choi, J. K. Lee, K. H. Song, K. Song, S. O. Kang and J. Ko, *Tetrahedron*, 2007, **63**, 1553.

9 B. Jędrzejewska, J. Kabatc, M. Pietrzak and J. Pączkowski, *Dyes Pigm.*, 2003, **58**, 47.

10 J. J. Li and E. J. Corey. *Name Reactions in Heterocyclic Chemistry*, Wiley-Interscience, Hoboken, N.J., 2005.

11 B. H. Yang and S. L. Buchwald, *J. Organomet. Chem.*, 1999, **576**, 125.

12 (*a*) J. Clayden, *Organolithiums: Selectivity for Synthesis*, Pergamon: Amsterdam, Boston, 1st edn, 2002; (*b*) J. A. Joule and K. Mills, *Heterocyclic Chemistry*, Blackwell Science, Malden, MA, 2000.

13 E. Runge and E. K. U. Gross, *Phys. Rev. Lett.*, 1984, **52**, 997.

14 (*a*) A. D. Becke, *J. Chem. Phys.*, 1993, **98**, 1372; (*b*) C. Lee, W. Yang and R. G. Parr, *Phys. Rev. B*, 1988, **37**, 785.

15 (*a*) M. Smith, J. March and J. March. *March's Advanced Organic Chemistry: Reactions, Mechanisms, and Structure*, Wiley, New York, 5th edn, 2001; (*b*) P. Y. Bruice *Organic Chemistry*, Prentice Hall, Upper Saddle River, N.J., 3rd edn, 2001.

16 (*a*) P. R. Varanasi, A. K. Y. Jen, J. Chandrasekhar, I. N. N. Namboothiri and A. Rathna, *J. Am. Chem. Soc.*, 1996, **118**, 12443; (*b*) I.-Y. Wu, J. T. Lin, J. Luo, C.-S. Li, C. Tsai, Y. S. Wen, C.-C. Hsu, F.-F. Yeh and S. Liou, *Organometallics*, 1998, **17**, 2188.

17 J. Zhang, H.-B. Li, S.-L. Sun, Y. Geng, Y. Wu and Z.-M. Su, *J. Mater. Chem.*, 2012, **22**, 568.

18 N. N. Matsuzawa, A. Ishitani, D. A. Dixon and T. Uda, *J. Phys. Chem. A*, 2001, **105**, 4953.

19 (*a*) K. Hara, Y. Dan-oh, C. Kasada, Y. Ohga, A. Shinpo, S. Suga, K. Sayama and H. Arakawa, *Langmuir*, 2004, **20**, 4205; (*b*) P. V. Kamat, *Chem. Rev.*, 1993, **93**, 267; (*c*) K.-M. Lee, V. Suryanarayanan, K.-C. Ho, K. R. Justin Thomas and J. T. Lin, *Sol. Energy Mater. Sol. Cells*, 2007, **91**, 1426.

20 X. Ren, Q. Feng, G. Zhou, C.-H. Huang and Z.-S. Wang, *J. Phys. Chem. C*, 2010, **114**, 7190.

21 S. Roquet, A. Cravino, P. Leriche, O. Alévêque, P. Frère and J. Roncali, *J. Am. Chem. Soc.*, 2006, **128**, 3459.

22 A. Hagfeldt and M. Graetzel, *Chem. Rev.*, 1995, **95**, 49.

23 N. J. Cherepy, G. P. Smestad, M. Grätzel and J. Z. Zhang, *J. Phys. Chem. B*, 1997, **101**, 9342.

24 R. Katoh, A. Furube, T. Yoshihara, K. Hara, G. Fujihashi, S. Takano, S. Murata, H. Arakawa and M. Tachiya, *J. Phys. Chem. B*, 2004, **108**, 4818.

25 (*a*) L. M. Peter, N. W. Duffy, R. L. Wang and K. G. U. Wijayantha, *J. Electroanal. Chem.*, 2002, **524–525**, 127; (*b*) A. Usami, S. Seki, Y. Mita, H. Kobayashi, H. Miyashiro and N. Terada, *Sol. Energy Mater. Sol. Cells*, 2009, **93**, 840.

26 Y. Liang, B. Peng and J. Chen, *J. Phys. Chem. C*, 2010, **114**, 10992.

27 T. Marinado, K. Nonomura, J. Nissfolk, M. K. Karlsson, D. P. Hagberg, L. Sun, S. Mori and A. Hagfeldt, *Langmuir*, 2009, **26**, 2592.